Original article

MOLECULAR METABOLISM

Opening of the mitochondrial permeability transition pore links mitochondrial dysfunction to insulin resistance in skeletal muscle*

E.P. Taddeo [1], R.C. Laker [2,3], D.S. Breen [1], Y.N. Akhtar [2,3], B.M. Kenwood [1], J.A. Liao [1], M. Zhang [2,3], D.J. Fazakerley [5], J.L. Tomsig [1], T.E. Harris [1], S.R. Keller [1], J.D. Chow [1], K.R. Lynch [1,4], M. Chokki [10], J.D. Molkentin [9], N. Turner [8], D.E. James [5,6,7], Z. Yan [1,2,3,*], K.L. Hoehn [1,2,3,4,*]

ABSTRACT

Insulin resistance is associated with mitochondrial dysfunction, but the mechanism by which mitochondria inhibit insulin-stimulated glucose uptake into the cytoplasm is unclear. The mitochondrial permeability transition pore (mPTP) is a protein complex that facilitates the exchange of molecules between the mitochondrial matrix and cytoplasm, and opening of the mPTP occurs in response to physiological stressors that are associated with insulin resistance. In this study, we investigated whether mPTP opening provides a link between mitochondrial dysfunction and insulin resistance by inhibiting the mPTP gatekeeper protein cyclophilin D (CypD) *in vivo* and *in vitro*. Mice lacking CypD were protected from high fat diet-induced glucose intolerance due to increased glucose uptake in skeletal muscle. The mitochondria in CypD knockout muscle were resistant to diet-induced swelling and had improved calcium retention capacity compared to controls; however, no changes were observed in muscle oxidative damage, insulin signaling, lipotoxic lipid accumulation or mitochondrial bioenergetics. *In vitro*, we tested 4 models of insulin resistance that are linked to mitochondrial dysfunction in cultured skeletal muscle cells including antimycin A, C_2-ceramide, ferutinin, and palmitate. In all models, we observed that pharmacological inhibition of mPTP opening with the CypD inhibitor cyclosporin A was sufficient to prevent insulin resistance at the level of insulin-stimulated GLUT4 translocation to the plasma membrane. The protective effects of mPTP inhibition on insulin sensitivity were associated with improved mitochondrial calcium retention capacity but did not involve changes in insulin signaling both *in vitro* and *in vivo*. In sum, these data place the mPTP at a critical intersection between alterations in mitochondrial function and insulin resistance in skeletal muscle.

Keywords Glucose; Insulin resistance; Mitochondrial dysfunction; Mitochondrial permeability transition pore; Cyclophilin D; Skeletal muscle

1. INTRODUCTION

Skeletal muscle tissue has an important role in whole body glucose homeostasis by increasing glucose clearance from the blood in response to insulin. Therefore, insulin resistance in skeletal muscle is a contributing factor to glucose intolerance and type 2 diabetes. Risk factors for skeletal muscle insulin resistance include aging and obesity; however, the molecular mechanisms are unclear. Current evidence links aging and obesity to insulin resistance in skeletal muscle *via* correlations with mitochondrial dysfunction, aberrant lipid accumulation, and oxidative stress [1–6]. For example, physiological studies in both humans and rodents demonstrate that acute lipid infusion or chronic consumption of a high fat diet (HFD) is sufficient to promote skeletal muscle insulin resistance concomitant with lipid accumulation in muscle and/or mitochondrial dysfunction [7–10]. Furthermore, skeletal muscle of young insulin resistant pre-diabetic patients that are non-obese also demonstrates mitochondrial dysfunction and aberrant lipid accumulation [11]. These data led the authors to speculate that mitochondrial

[1]Department of Pharmacology, University of Virginia, Charlottesville, VA 22908, USA [2]Department of Medicine, University of Virginia, Charlottesville, VA 22908, USA [3]Robert M. Berne Cardiovascular Research Center, University of Virginia, Charlottesville, VA 22908, USA [4]Emily Couric Clinical Cancer Center, University of Virginia, Charlottesville, VA 22908, USA [5]Diabetes and Obesity Program, Garvan Institute of Medical Research, 384 Victoria St., Darlinghurst, NSW 2010, Australia [6]School of Medical Sciences, University of New South Wales, Sydney, NSW, Australia [7]School of Biotechnology and Biomolecular Sciences, University of New South Wales, Sydney, NSW, Australia [8]Department of Pharmacology, University of New South Wales, Sydney, NSW, Australia [9]Department of Pediatrics, University of Cincinnati, Cincinnati Children's Hospital Medical Center, Howard Hughes Medical Institute, Cincinnati, OH, USA [10]Teijin Pharma Limited, 4-3-2, Asahigaoka, Hino, Tokyo 191-8512, Japan

*Corresponding authors at: Department of Pharmacology, University of Virginia, Charlottesville, VA 22908, USA. Tel.: +1 434 924 2577.
Email: zy3m@virginia.edu (Z. Yan), klh8st@virginia.edu (K.L. Hoehn).

Abbreviations: MPTP, mitochondrial permeability transition pore; CYPD, cyclophilin D; HFD, high fat diet; LFD, low fat diet; WT, wild type; KO, knockout; CSA, cyclosporin A; BKA, bongkrekic acid; $O_2^{\bullet}$, superoxide; [^{3}H]-2-DOG, [^{3}H]-2-deoxyglucose; Rg′, rate of glucose transport; FFA, free fatty acid; DAG, diacylglycerol; TEM, transmission electron microscopy; PDH, pyruvate dehydrogenase; PDH_a, active PDH; PDH_t, total PDH; MCAD, medium chain acyl-CoA dehydrogenase; β-HAD, β-hydroxyacyl-CoA dehydrogenase; PM, plasma membrane; ANT, adenine nucleotide translocator; VDAC, voltage-dependent anion channel; HK2, hexokinase 2; ETC, electron transport chain; OXPHOS, oxidative phosphorylation; MnSOD, mitochondrial manganese superoxide dismutase; MIRKO, muscle insulin receptor knockout; MHC, myosin heavy chain; TBARS, thiobarbituric acid reactive substances

Received November 8, 2013 • Accepted November 14, 2013 • Available online 26 November 2013

http://dx.doi.org/10.1016/j.molmet.2013.11.003

inefficiency may promote lipotoxic lipid accumulation to drive skeletal muscle insulin resistance. Together, these studies and others [12] have identified an association between mitochondrial dysfunction and insulin resistance, but cause–effect relationships remain to be proven [12]. Further work is required to determine the molecular mechanisms linking skeletal muscle mitochondria to insulin sensitivity.

We have previously demonstrated that acute induction of mitochondrial superoxide ($O_2^{\bullet}$) in skeletal muscle myotubes with the mitochondrial electron transport chain (ETC) inhibitor antimycin A was sufficient to cause insulin resistance [2]. This mechanism of insulin resistance was prevented by overexpression of mitochondrial manganese superoxide dismutase (MnSOD), treatment with mitochondrial $O_2^{\bullet}$ scavengers, and inhibition of the ETC with stigmatellin at a site upstream of antimycin A. Collectively, this experiment demonstrated that mitochondrial $O_2^{\bullet}$, but not altered ATP production, is sufficient to drive insulin resistance in skeletal muscle. However, it also revealed a gap in knowledge concerning the mechanism whereby membrane impermeable mitochondrial $O_2^{\bullet}$ triggers insulin resistance, a process that occurs in the cytoplasm and at the plasma membrane (PM) [13,14]. To explore this mechanism we investigated a role for the mitochondrial permeability transition pore (mPTP). The mPTP is a multi-protein complex that spans both mitochondrial membranes and allows the passage of molecules less than 1500 Da between the cytoplasm and mitochondrial matrix. Importantly, the mPTP is triggered to open by mitochondrial $O_2^{\bullet}$ and other factors linked to insulin resistance including mitochondrial calcium overload [15–18]. Under normal physiological conditions, transient opening of the mPTP releases ions and metabolites from the mitochondrial matrix in order to maintain proper homeostasis [16,17,19–21]. To investigate whether opening of the mPTP is required for insulin resistance, we targeted the mitochondrial matrix peptidyl-prolyl *cis-trans* isomerase cyclophilin D (CypD). CypD regulates mPTP opening by directly binding to pore constituent proteins, and inhibition of CypD decreases the probability of mPTP opening [18,19,21]. Based on these data, we investigated whether the genetic or pharmacological inhibition of CypD would protect from insulin resistance.

2. MATERIALS AND METHODS

2.1. Cell culture

Maintenance and differentiation of L6 rat skeletal muscle cells expressing HA-tagged GLUT4 was performed as described [2,22]. Differentiation of myoblasts into myotubes was induced by culturing cells in MEM-α containing 2% (v/v) horse serum and 1% (v/v) penicillin–streptomycin. L6 myotubes were treated with specified drugs for the durations and concentrations noted in the figure legends. Ferutinin, bongkrekic acid (BKA), cyclosporin A (CsA), antimycin A, C_2-ceramide, and bovine serum albumin (BSA) were purchased from Sigma Aldrich (St. Louis, MO).

2.2. GLUT4 translocation assays

GLUT4 translocation assays were performed as previously described [2] in L6 myotubes treated with either 150 μM palmitic acid conjugated to BSA or ethanol (control) in DMEM. Palmitate–BSA complexes were made by combining BSA (20% BSA stock) and palmitic acid (200 mM palmitic acid stock) in DMEM while vortexing at low speed at 50 °C. The palmitate:BSA or ethanol:BSA (vehicle control) solutions were heated at 50 °C in a water bath for 20 min, then cooled to 37 °C for 15 min and diluted in DMEM to the final concentrations indicated. The diluted solutions were sterile filtered through a 0.45 μm PVDF membrane prior to treatment of myotubes.

2.3. Western blotting

Following drug treatment, cells were washed twice with ice-cold phosphate-buffered saline (PBS) and lysed with HEPES–EDTA–Sucrose lysis buffer (250 mM sucrose, 20 mM HEPES pH 7.4, and 1 mM EDTA) containing 2% sodium dodecyl sulfate (SDS). Whole cell lysates were cleared of insoluble material by centrifugation [22]. Quadriceps (~20 mg) were homogenized in 20 × volumes (~400 μL) of radioimmunoprecipitation assay (RIPA) buffer [150 mM NaCl, 10 mM nonyl phenoxypolyethoxylethanol (NP)-40, 0.5% sodium deoxycholate, 0.1% SDS, 50 mM Tris pH 7.5] containing protease inhibitors (Roche) and phosphatase inhibitors (2 mM Na-orthovanadate, 1 mM Na-pyrophosphate, 10 mM Na-fluoride, 250 nM microcystin LR). Homogenates were sonicated, rotated at 4 °C for 1 h and centrifuged at 16,000 × *g* at 4 °C for 10 min. Lysates were diluted in 4 × Laemmli buffer and denatured at 65 °C for 5 min. Cellular proteins (20 μg) were resolved on 10% SDS-polyacrylamide gels or AnykD pre-cast gels (Bio-Rad Laboratories, Hercules, CA) and electro-transferred overnight onto nitrocellulose membranes. Equal protein loading was confirmed by Ponceau staining. Protein expression was detected with the following antibodies: phospho-Akt S473, total Akt, phospho-GSK3β S9, total GSK3β, hexokinase 2, total pyruvate dehydrogenase (PDH) and glyceraldehyde 3-phosphate dehydrogenase (GAPDH) (Cell Signaling, Beverly, MA), phospho-insulin receptor (IR)/insulin-like growth factor 1 receptor (IGF1R) Y1158/Y1162/Y1163 (Millipore, Billerica, MA), CypD (Mitosciences, Eugene, OR), 14-3-3 (Santa Cruz Biotechnology, Dallas, Texas), phospho-PDH S293 E1α (Novus Biologicals, Littleton, CO), GLUT4 R82 (generously provided by Dr. Thurl Harris, University of Virginia Department of Pharmacology), myosin heavy chain (MHC) I (BA-F8) and MHC IIa (sc-71) (generous gifts from Dr. Zhen Yan, University of Virginia Robert M. Berne Cardiovascular Research Center). Primary antibodies were detected using goat anti-mouse IgG (DyLight 800 conjugate) or goat anti-rabbit IgG (DyLight 680 conjugate) polyclonal secondary antibodies. Membranes were visualized, and protein band intensities quantified, using the LI-COR ODYSSEY System and software (LI-COR, Lincoln, NE, USA).

2.4. Animals

Food and water were provided *ad libitum* until the date of study and all animal care was in compliance with NIH guidelines and the University of Virginia Animal Care and Use Committee. The high fat diet (45% kcal as fat) was purchased from Research Diets (D12451). Normal chow diet was purchased from Harlan Teklad (diet 7912). Animals were maintained on a 12/12 light/dark schedule at 68–72 °F and housed 4–5 per cage. The CypD KO mice were obtained from Dr. Jeffrey Molkentin [23] and maintained on an inbred C57BL/6 background as heterozygous breeding pairs. Glucose tolerance tests were performed on mice that were fasted for 5–6 h prior to intraperitoneal injection of glucose (1.5–2 g/kg). Blood glucose levels were monitored at indicated time points using an Accu-check II glucometer (Roche Diagnostics). Clearance of the glucose analog [^{3}H]-2-deoxyglucose ([^{3}H]-2-DOG) into glucose-6-phosphate and [U-^{14}C]-glucose into glycogen was measured in quadriceps muscles as described previously [2,24].

2.5. Serum and tissue analyses

Serum insulin was determined by ELISA (Crystal Chem, Downers Grove, IL). Non-esterified fatty acids were measured from serum samples by colorimetric assay (WAKO diagnostics, Osaka Japan). Transmission electron microscopy (TEM) was performed at the UVa EM facility using finely diced tibialis cranialis muscle fixed in 4% glutaraldehyde and 2.5% paraformaldehyde for 3 days prior to post-

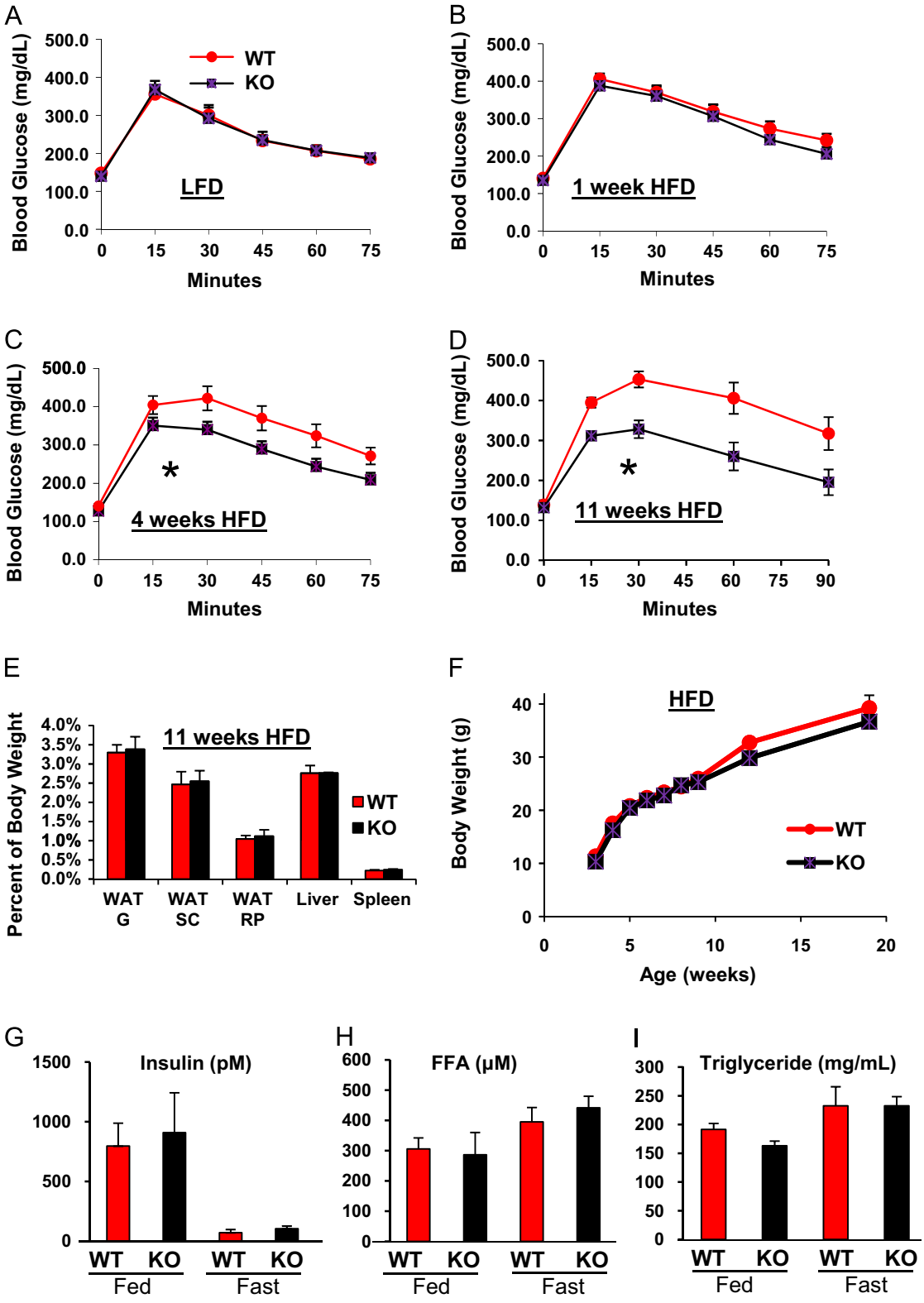

Figure 1: CypD KO mice are protected from HFD-induced glucose intolerance. (A–D) CypD knockout (KO) mice and wild type (WT) control littermates were fed a LFD until 8 weeks of age when they were switched to a 45% high fat diet (HFD) for up to 11 weeks. Glucose tolerance was tested at weeks 0 (LFD), 1, 4, and 11 of HFD (2 g/kg glucose in (A) and 1.5 g/kg in (B–D)); * represents a significant difference in integrated AUC ($p < 0.05$). (E and F) Gonadal, subcutaneous (inguinal), and retroperitoneal white adipose tissue (WAT) mass, liver mass, and total body mass were not statistically different between genotypes when fed a HFD diet for up to 11 weeks. Circulating insulin (G), free fatty acid (FFA) (H), and triglyceride (I) levels were similar between genotypes in either the fed or fasted states. Data are presented as means ± standard error of the mean (SEM). $n = 8–16$ for A–F and $n = 4–7$ for G–I.

fixation in osmium tetroxide. TEM images were taken using a JEOL 1230. Mitochondrial length in the TEM images was calculated with ImageJ using a standard size scale (600 pixels = 1 μm). At least 170 intermyofibrillar and ≥ 90 subsarcolemmal mitochondria from 2 animals per genotype were quantified. Only mitochondria fully contained within the borders of the TEM images were included in the analysis.

2.6. Measurement of sphingolipids, glycerolipids and phospholipid derivatives

Powdered quadriceps muscles (~15 mg) were weighed and homogenized using a Polytron (Brinkman Instruments, Westbury, NY) in 1 mL acidified methanol (0.1 N HCl) containing internal standard cocktails for sphingolipids (containing 0.5 nmol each: C_{17}-ceramide, C_{12}-glucosylceramide, C_8-dihydroceramide, and C_{12}-sphingomyelin) and glycerolipids (0.1 nmol each of C_{15}-diacylglycerol and C_{17}-lysophosphatidic acid). The homogenate was divided into two 500 μL aliquots for extraction of sphingolipids and glycerolipids/phospholipid derivatives.

To measure sphingolipids, 250 μL of chloroform was added to the homogenate, and the homogenate was incubated overnight at 48 °C. After cooling to room temperature, 200 μL of 0.1 M KOH in methanol was added, and the samples were incubated at 37 °C for 2 h. Lipids were neutralized with 17 μL of glacial acetic acid and centrifuged at 5000 × *g* for 10 min to pellet debris. One milliliter of chloroform and 2 mL of millipure H_2O were added to the supernatant, vortexed, and centrifuged at 1500 × *g* for 15 min to separate the organic and aqueous phases. The organic phase was dried under nitrogen prior to resuspension in mobile phase solvent containing 97% acetonitrile, 2% methanol, and 1% formic acid (v/v/v) supplemented with 5 mM ammonium formate. Samples were subjected to normal phase LC/MS/MS using a using a triple quadrupole mass spectrometer (Applied Biosystems 4000 Q-Trap) coupled to a Shimadzu LC-20AD LC system equipped with a Supelcosil LC NH2 column (50 cm × 2.1 mm, 3 μm) and a multiple reaction monitoring scheme for naturally occurring species of ceramide, glucosylceramide, and sphingomyelin. Data acquisition was performed as we have described [25], and quantification was carried out by measuring peak areas for each analyte using Analyst 1.5.1 software. Recovery was assessed using internal standards, and values were normalized to tissue weight and dilution.

To measure glycerolipids and phospholipid derivatives, 250 μL of chloroform was added to 500 μL homogenate, and the homogenate was incubated on ice for 60 min. Chloroform (250 μL) and 0.2 M NaOH in H_2O (250 μL) was added to the samples. The samples were vortexed, centrifuged for 5 min at 1000 × *g* and the organic phase was extracted and dried under nitrogen. Dried lipids were resuspended in mobile phase solvent (69% methanol, 31% H_2O, 10 mM ammonium acetate) for LC/MS/MS with appropriate Reverse Phase chromatographic columns. Diacylglycerols (DAGs), phosphatidylcholines (PCs) and phosphatidylethanolamines (PEs) were analyzed in positive mode after separation in a Discovery (Supelco) C18 column (50 mm × 2.1 mm, 5 μm bead size). Mobile phase A consisted of 69% methanol, 31% H_2O, 10 mM ammonium acetate; and mobile phase B consisted of 1:1 ethanol:isopropanol (v/v) supplemented with 10 mM ammonium acetate. The solvent gradient was as follows: 1 min 100% solvent A, a linear gradient to reach 100% solvent B at 9 min, 1 min 100% solvent B, 2 min 100% solvent A. Total flow was 0.75 ml/min. DAGs were analyzed by monitoring product ions generated by neutral loss of ammoniated acyl groups [RCOOH + NH_3] from DAGs ammonium adducts $[M+NH_4]^+$ as previously described [26]. PCs were analyzed by the production of the *m/z* 184 phosphocholine ion, whereas PEs were analyzed by monitoring the product ions obtained after the loss of a *m/z* 141.1 neutral fragment [27]. Phosphatidic acids (PAs), lisophosphatidic acids (LPAs), and phosphatidylserines (PSs) were analyzed in negative mode after separation in a Nucleodur (Macherey Nagel) C8 column (125 mm × 2 mm, 5 μm bead size). Mobile phase A consisted of 75% methanol, 25% H_2O, 0.1% formic acid, and 1 mM ammonium acetate. Mobile phase B consisted of 80% methanol, 20% chloroform, 0.1% formic acid, and 1 mM ammonium acetate. The solvent gradient was as follows: 1 min 100% solvent A, 1 min 65% solvent B, a linear gradient to reach 77% solvent B at 7 min, 3 min 100% solvent B, 2 min 100% solvent A. Total flow was 0.33 ml/min. LPAs were analyzed by the production of the *m/z* 153 glycerophosphate ion, PAs were analyzed by the production of an ion corresponding to the loss of an acyl chain (the most intense ion was used), and PSs were analyzed by monitoring the product ions obtained after the loss of a *m/z* 87.0 neutral fragment [28]. Optimal settings (DP, EP, CE, and CXP voltages; Ion Spray voltage, and gas flows) were obtained by infusion of selected authentic phospholipids. Quantification was carried out by measuring peak areas for each analyte using Analyst 1.5.1. Recovery was assessed using appropriate internal standards. LPAs, PAs, PCs, PEs, and PSs were normalized to C_{17}-LPA, and DAGs were normalized to C_{15}-DAG. Total values were normalized to tissue weight and dilution factor.

2.7. Calcium retention capacity

Isolated mitochondria were obtained from gastrocnemius muscles. Muscle tissues were placed in 5 ml of ice-cold isolation buffer (in mM: 150 sucrose, 75 KCl, 50 Tris-base, 1 KH_2PO_4, 5 $MgCl_2$, 1 EGTA, 0.2% BSA, pH 7.4) with 5 mg/ml of nagarse (Sigma P8038) for 1 min. Tissue was homogenized using a polytron homogenizer. Isolation buffer (15 mL) was further added and centrifuged at 700 × *g* for 10 min at 4 °C. The supernatant was then centrifuged at 10,000 × *g* for 10 min at 4 °C. The pellet obtained was resuspended in 15 mL of suspension buffer (in mM: 250 sucrose, 10 Tris-base, 0.1 EGTA, pH 7.4) and centrifuged at 8000 × *g* for 10 min at 4 °C. The mitochondrial pellet was then resuspended in 50 μL of suspension buffer. DC Protein Assay Kit (BioRad, USA) was used to measure protein concentration in the buffer. Mitochondria (15 μg) were suspended into a total volume of 100 μL using mitochondrial challenge buffer (in mM: 250 sucrose, 10 MOPS, 0.05 EGTA, 10 Pi-Tris, pH 7.4) with the addition of 50 mM of Na-succinate (Sigma S2378) and 10 μM rotenone (Sigma R8875). Calcium Green 5N (1 μM; Invitrogen C3737) was added and fluorescence was measured using an excitation/emission wavelength of 506/532 nm, respectively, in a FLUOstar omega plate reader (BMG Labtech). Calcium chloride (83 nmol/mg protein) was added at regular pulses as indicated.

2.8. Statistical analyses

Data were expressed as means ± standard error of the mean (SEM) of at least 3 independent experiments or animals per group. *p*-Values were calculated by two-tailed Student's *t*-test, one-way ANOVA with either Fisher's PLSD or Tukey's post-hoc test or two-way ANOVA with Sidak's post-hoc test. Statistical significance was set at $p < 0.05$.

3. RESULTS

3.1. CypD KO mice are resistant to diet-induced glucose intolerance and demonstrate improved skeletal muscle glucose uptake

To test the role of the mPTP in diet-induced insulin resistance, we fed whole-body CypD knockout (KO) mice and wild type (WT) littermate

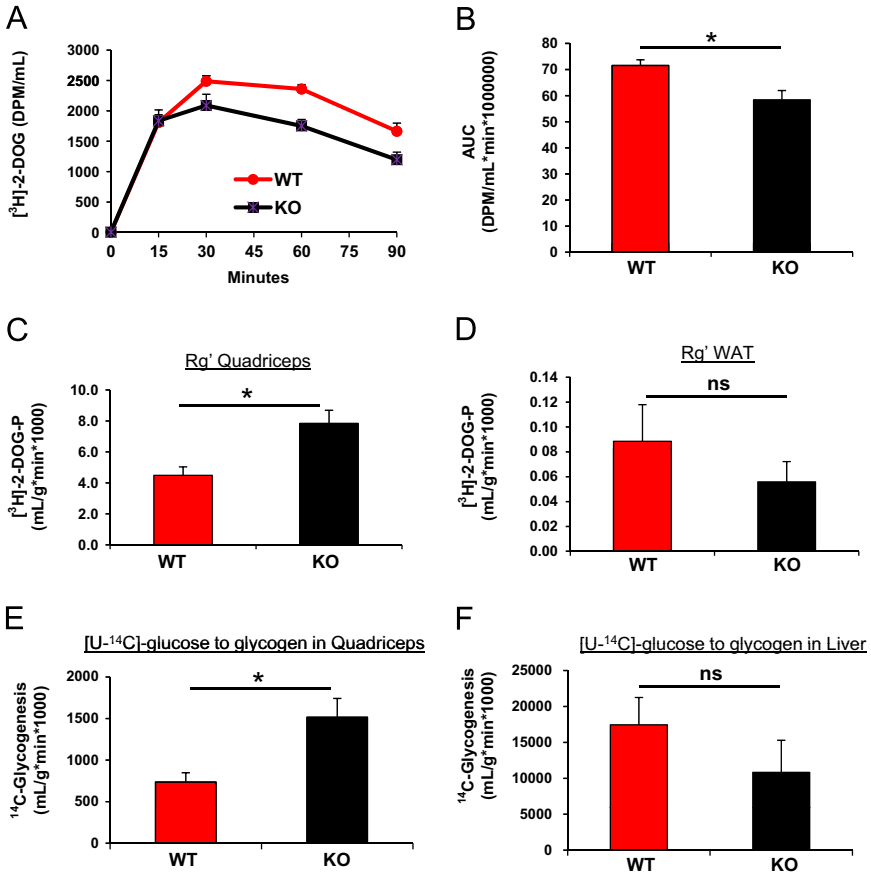

Figure 2: Improved skeletal muscle glucose clearance in CypD KO mice fed HFD for 11 weeks. (A) [^{3}H]-2-DOG tracer appearance and disappearance curves for each genotype. (B) The calculated AUC for each genotype. (C and D) The estimated rate of glucose transport (Rg') into quadriceps muscle and gonadal WAT as determined by phosphorylated-[^{3}H]-2-DOG normalized to tracer availability over time and tissue mass. (E and F) [U-^{14}C]-glucose storage as glycogen in quadriceps muscle and liver. Data are represented as means $\pm$ SEM of 9 WT and 8 KO. *$p < 0.05$. ns, not significant.

controls a low fat chow diet (LFD) or high fat diet (HFD) for a period of up to 11 weeks. Glucose tolerance tests were performed at weeks 1, 4, and 11 of HFD feeding. As shown in Figure 1A–D, WT mice had time-dependent impairment in glucose clearance when challenged with an intraperitoneal bolus of glucose, whereas CypD KO mice were largely protected from glucose intolerance. The improved glucose tolerance was not due to differences in adiposity (Figure 1E), body weight (Figure 1F and Supplemental Figure S1), or food intake (2.98 ± 0.10 and 2.88 ± 0.06 g/mouse/night for WT and CypD KO, respectively). Also, serum insulin, free fatty acid (FFA), or triglyceride levels were not statistically different between genotypes in either the fed or fasted states (Figure 1G–I). Therefore, these parameters were not underlying the improved glucose clearance observed in the CypD KO mice.

To determine the tissue type(s) that accounted for the increased glucose clearance, CypD KO and WT control mice fed a HFD for 11 weeks were administered a glucose bolus containing [U-^{14}C]-glucose and [^{3}H]-2-deoxyglucose ([^{3}H]-2-DOG) (Figure 2). The clearance of [^{3}H]-2-DOG from the circulation was significantly higher in the CypD KO mice compared to WT controls (Figure 2A and B). Analysis of tissue [^{3}H]-2-DOG-phosphate identified a 1.75-fold increase in glucose uptake in CypD KO quadriceps muscle (Figure 2C, $p < 0.01$) compared to WT controls, with no significant changes in glucose uptake in adipose tissue (Figure 2D, $p = 0.12$). Skeletal muscle tissue of CypD KO mice also utilized more glucose for glycogen storage compared to WT controls, as determined by a 2.1-fold increase in the incorporation of [U-^{14}C]-glucose into glycogen (Figure 2E, $p < 0.05$). In contrast, hepatic glycogen synthesis was not significantly different between CypD KO and WT mice (Figure 2F, $p = 0.24$). These data point to an important role for skeletal muscle, but not adipose or liver tissues, in whole body glucose clearance in CypD KO mice.

3.2. Enhanced skeletal muscle glucose utilization in CypD KO mice is independent of insulin signaling and lipid accumulation

To further investigate the mechanism underlying improved glucose tolerance (increased glucose uptake and storage) in skeletal muscle from CypD KO mice, we evaluated the expression of proteins that regulate glucose metabolism and insulin signaling in this tissue. After 11 weeks of HFD, the phosphorylation of Akt (S473) and GSK3β (S9), and the expression of GLUT4, hexokinase 2 (HK2) and pyruvate dehydrogenase (PDH) were not altered in skeletal muscle from CypD KO mice compared with WT mice (Figure 3A–D and Supplemental Figures S2 and S3).

Lipid accumulation in skeletal muscles can lead to lipotoxicity and is associated with insulin resistance. We therefore measured lipid accumulation in skeletal muscle from high fat-fed mice injected with glucose. Mice were harvested 90 min after glucose injection (1.5 g/kg) as this time point correlates with the period during which we observe the improved glucose uptake and metabolism (Figure 2). However, there were no observable differences in the accumulation of ceramides, diacylglycerols (Figure 3E and F), or other sphingolipids, glycerolipids or phospholipid derivatives in skeletal muscle from CypD KO and WT mice (Supplemental Figures S4 and S5).

The proportion of oxidative skeletal muscle fibers is indicative of insulin sensitivity in humans, as insulin resistant subjects have fewer type I oxidative

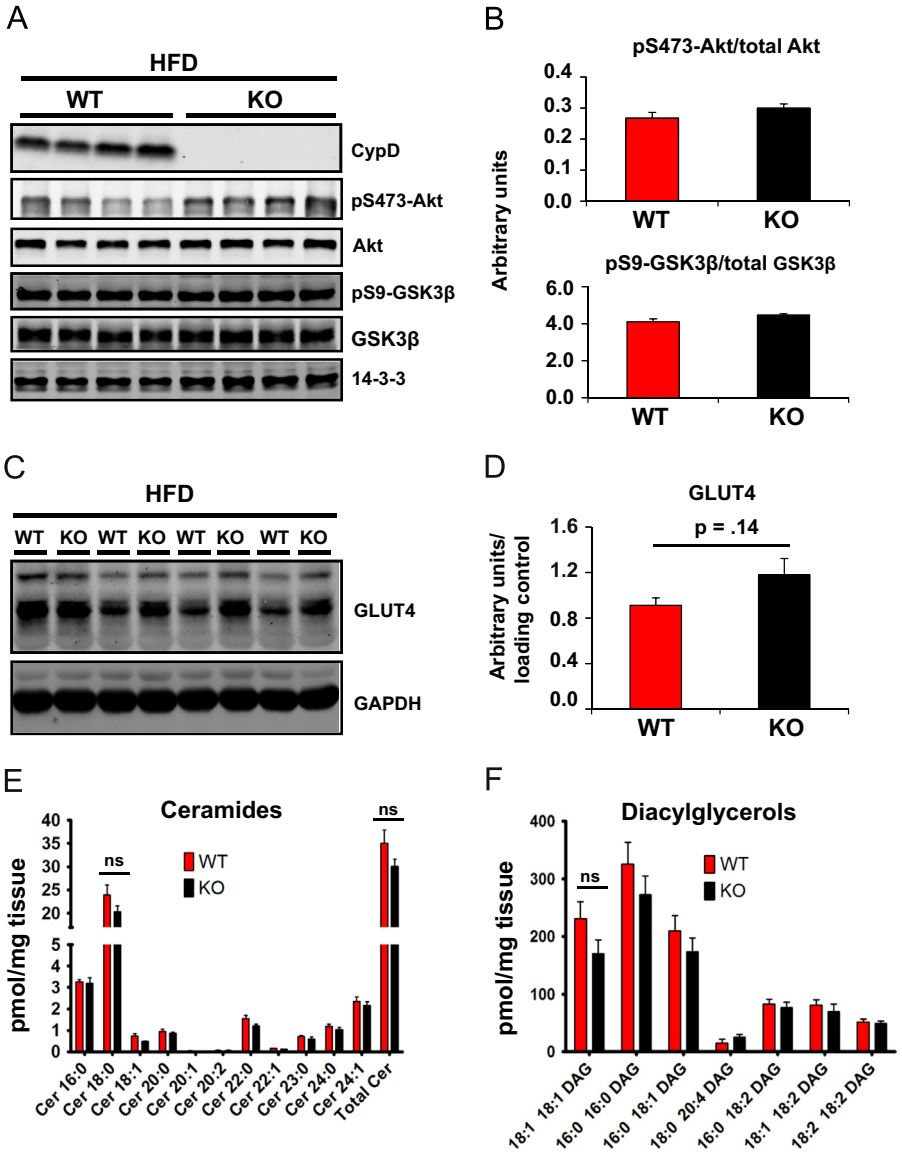

Figure 3: Insulin signaling, GLUT4 protein expression, and lipid analysis of skeletal muscle from mice fed a HFD for 11 weeks. (A) Western blots for CypD, phospho-S473 Akt, total Akt, phospho-S9 GSK3β and total GSK3β in mixed quadriceps muscles. Expression of 14-3-3 was used as a loading control. (B) Quantification of phospho/total Akt and phospho/total GSK3β immunoblots. (C) Western blot of GLUT4 protein expression in quadriceps muscle. GAPDH served as a loading control. (D) Quantification of normalized GLUT4 expression. (E and F) Ceramide and diacylglycerol levels in quadriceps. Results are displayed as means ± SEM, $n \geq 3$, ns, not significant.

muscle fibers and more type II glycolytic fibers [29]. However, we found that the ratio of type I oxidative fibers to type II glycolytic fibers was similar between genotypes (Supplemental Figures S6 and S7). Furthermore, the level of Thiobarbituric Acid Reactive Substances (TBARS) and protein carbonyls, which are indicative of skeletal muscle oxidative damage, were not different between CypD KO and WT mice on HFD (Supplemental Figure S8).

In sum, these data indicate that the mechanism whereby CypD ablation protects from diet-induced glucose intolerance is likely downstream or independent of metabolic enzyme expression, signal transduction defects, lipotoxicity, and changes in either skeletal muscle fiber composition or oxidative damage.

3.3. Improved mitochondrial morphology and calcium retention capacity in CypD KO skeletal muscle

Mitochondrial swelling is reported in skeletal muscles of insulin resistant mice fed a HFD [10]. To determine whether mitochondrial swelling was altered in skeletal muscle lacking CypD, we analyzed mitochondrial morphology by transmission electron microscopy (TEM). Consistent with previous reports [10], we observed that the mitochondria within skeletal muscle fibers of WT mice fed a HFD were vacuolated and swollen in both intermyofibrillar and subsarcolemmal muscle regions. In contrast, CypD KO skeletal muscle did not show any mitochondrial swelling or accumulation of damaged organelles (Figure 4A–D). However, these morphological differences in skeletal muscle mitochondria between WT and CypD KO mice were not accompanied by changes in mitochondrial size (Figure 4E), or activities of skeletal muscle oxidative enzymes including mitochondrial citrate synthase and the β-oxidation enzymes medium chain acyl-CoA dehydrogenase (MCAD) and β-hydroxyacyl-CoA dehydrogenase (β-HAD) (Supplemental Figure S9). Similarly, enzyme activities of ETC complexes I, II, and IV were comparable in skeletal muscle from CypD KO and WT mice (Supplemental Figure S9). Mitochondria isolated from quadriceps muscles of CypD KO and WT

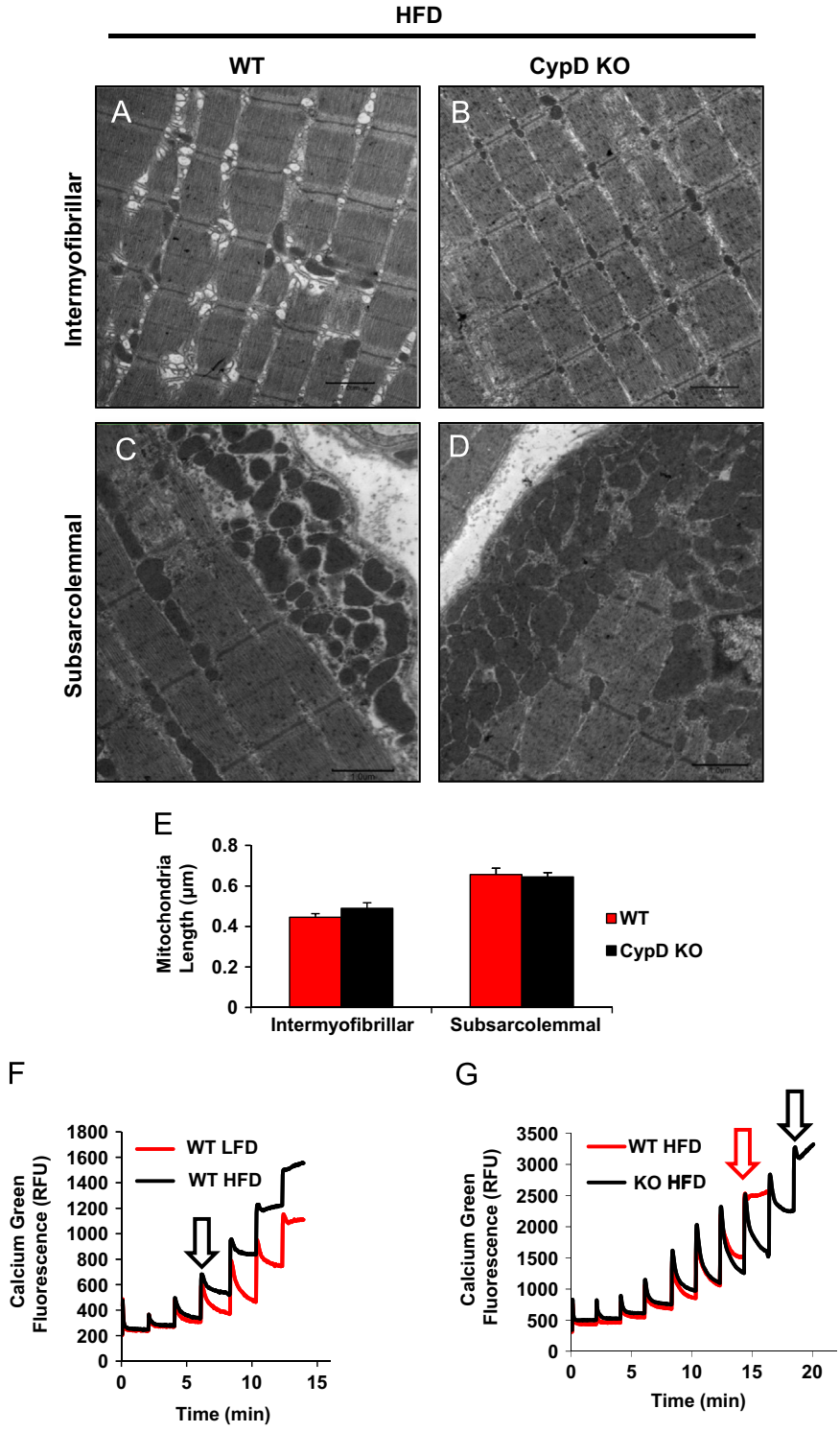

Figure 4: Skeletal muscle morphology and mitochondrial calcium retention capacity in WT and CypD KO mice. (A–D) Representative TEM images (10,000 × magnification) of intermyofibrillar and subsarcolemmal mitochondria in tibialis cranialis muscle from WT and CypD KO mice fed a HFD for 29 weeks. Scale bar equals 1 μm. (E) Quantification of mitochondrial length in tibialis cranialis muscles. Lengths from ≥ 170 mitochondria per genotype (intermyofibrillar) or ≥ 90 mitochondria per genotype (subsarcolemmal) were quantified in TEM images using ImageJ. (F) Representative trace from three calcium retention capacity assays of mitochondria isolated from gastrocnemius muscles of WT mice fed a LFD or HFD for 10 weeks. (G) Representative trace from three calcium retention capacity assays comparing WT and CypD KO mice fed HFD for 10 weeks. Arrows indicate calcium-induced mPTP opening.

mice also showed similar native ETC complex content and supramolecular assembly (Supplemental Figure S10), PDH activity (Supplemental Figure S3) and bioenergetic function (Supplemental Figure S11). In contrast, HFD feeding was associated with a decrease in skeletal muscle mitochondrial calcium retention capacity in WT mice (Figure 4F), an effect that was rescued by deletion of CypD (Figure 4G). These

results indicate that CypD ablation may improve skeletal muscle glucose uptake by preserving mitochondrial morphology and calcium handling in insulin resistant skeletal muscle.

3.4. Inhibition of mPTP opening prevents multiple models of insulin resistance *in vitro*

We next sought to determine if mPTP opening was sufficient or necessary to induce insulin resistance, as determined by inhibition of insulin-stimulated GLUT4 trafficking to the PM, an endpoint of the insulin signaling pathway. We tested 2 well-documented mechanisms of mPTP opening including mitochondrial calcium overload [30] and mitochondrial $O_2^{\bullet}$ production [16] in cultured L6 myotubes. Mitochondrial calcium overload was induced by 30 min treatment with the ionophore ferutinin [31,32]. Ferutinin treatment caused dose-dependent inhibition of insulin-stimulated GLUT4 trafficking to the PM that was reversible with either of the mPTP inhibitors cyclosporin A (CsA) or bongkrekic acid (BKA) (Figure 5A). CsA inhibits CypD and calcineurin, whereas BKA inhibits another mPTP regulatory component, the adenine nucleotide translocator (ANT). Since CsA is a dual inhibitor of both CypD and calcineurin, we confirmed that the calcineurin inhibitor FK506 did not protect myotubes from ferutinin-induced mPTP opening and insulin resistance (Supplemental Figure S12). Ferutinin-induced insulin resistance did not affect insulin signaling through Akt, nor was signaling altered by CsA or BKA (Figure 5B).

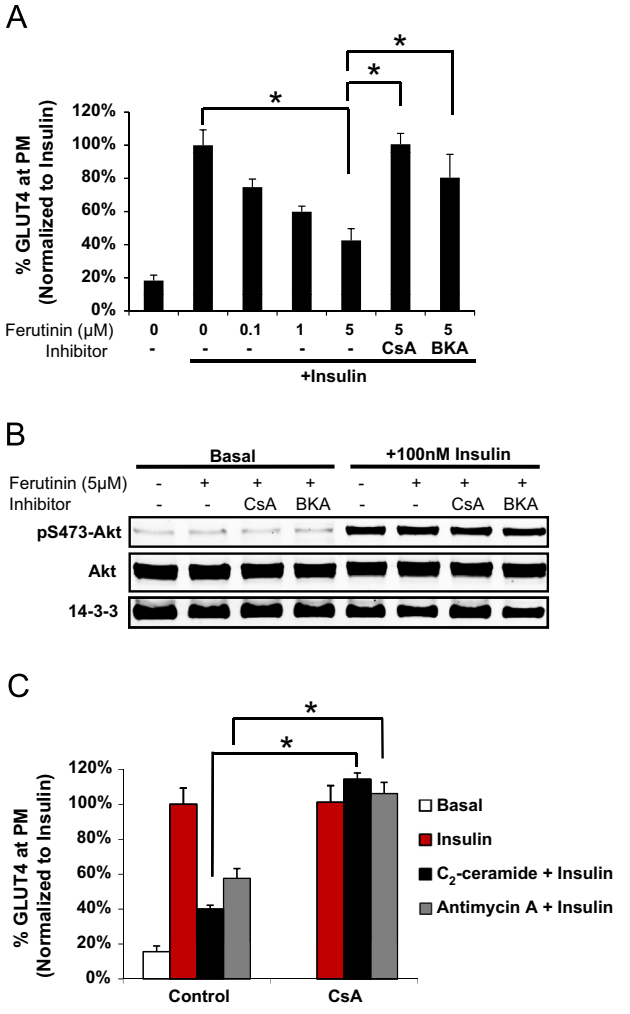

Figure 5: mPTP opening drives insulin resistance *in vitro*. (A) Insulin-stimulated GLUT4 translocation was analyzed in L6 myotubes treated for 30 min with increasing concentrations of ferutinin (0.1 μM, 1 μM, and 5 μM) in the absence or presence of a 10 min pretreatment with mPTP inhibitors CsA (1 μg/mL) or BKA (10 μM). (B) Akt phosphorylation in basal or insulin-stimulated L6 myotubes treated with or without 5 μM ferutinin in the absence or presence of 1 μg/mL CsA or 10 μM BKA. Representative Western blots from three individual experiments are shown. (C) GLUT4 translocation assay after a 30 min treatment with 100 nM C_2-ceramide or 50 nM antimycin A, with or without 10 min pretreatment with 1 μg/mL CsA, $n=3$. Results are displayed as means ± SEM, $^*p < 0.05$.

Here we have previously demonstrated that the mitochondrial complex III inhibitor antimycin A is sufficient to promote mitochondrial $O_2^{\bullet}$ production and cause insulin resistance [2]. Here we show that antimycin A-induced insulin resistance requires mPTP opening, as CsA fully protected L6 myotubes from defects in GLUT4 trafficking caused by antimycin A (Figure 5C). Antimycin A-induced insulin resistance occurred without significant changes in cellular ATP content (Supplemental Figure S13). Previously, we have validated that antimycin A-induced insulin resistance is due to $O_2^{\bullet}$ rather than mitochondrial inhibition because it is reversible by overexpression of MnSOD [2]. To confirm the requirement of the mPTP for $O_2^{\bullet}$-induced insulin resistance, we also tested C_2-ceramide, which is an inducer of mitochondrial $O_2^{\bullet}$ [33] and promotes insulin resistance [34]. As shown in Figure 5C, CsA also completely prevented insulin resistance caused by C_2-ceramide.

Finally, we and others have demonstrated that low-dose (150 μM) palmitate induces insulin resistance in L6 myotubes at the level of GLUT4 trafficking to the PM, without disrupting insulin signaling [2,22]. Here we show that palmitate treatment reduced mitochondrial calcium retention capacity (Figure 6A) and impaired insulin-stimulated GLUT4 trafficking to the PM (Figure 6B). Treatment of myotubes with CsA prevented palmitate-induced insulin resistance at the level of GLUT4 translocation and improved mitochondrial calcium retention capacity (Figure 6A and B). Overall, these data identify that CypD-dependent opening of the mPTP is required for multiple models of skeletal muscle insulin resistance *in vitro* and *in vivo* as outlined in Figure 6C.

4. DISCUSSION

Abnormal mitochondrial structure and/or function are correlated with insulin resistance in skeletal muscle. In the present study, we investigated whether the mPTP represents a link between mitochondrial dysfunction and insulin resistance. The rationale for investigating the mPTP included (1) the close proximity of the mPTP to the source of mitochondrial $O_2^{\bullet}$ production in the mitochondrial inner membrane; (2) opening of the mPTP can be rapid and reversible, and is triggered by insults that are associated with insulin resistance including mitochondrial $O_2^{\bullet}$ and mitochondrial calcium overload; and (3) mPTP opening serves as a potential means of communication between mitochondrial stress and insulin-stimulated GLUT4 translocation to the PM and glucose uptake into the cytoplasm. We identified that genetic deletion of CypD, which decreases the probability of mPTP opening [18–21], protected mice from HFD-induced glucose intolerance and increased glucose uptake specifically in skeletal muscle. The increased glucose uptake in skeletal muscle was associated with preserved mitochondrial morphology and improved mitochondrial calcium handling. In cultured muscle cells, we found that mitochondrial $O_2^{\bullet}$, mitochondrial calcium overload, and palmitate all require mPTP opening for induction of insulin resistance. These results position the mPTP at a critical intersection between alterations in mitochondrial function and insulin resistance in skeletal muscle.

It is intriguing that the improved glucose tolerance in high fat-fed CypD KO mice was associated with improved glucose uptake in skeletal

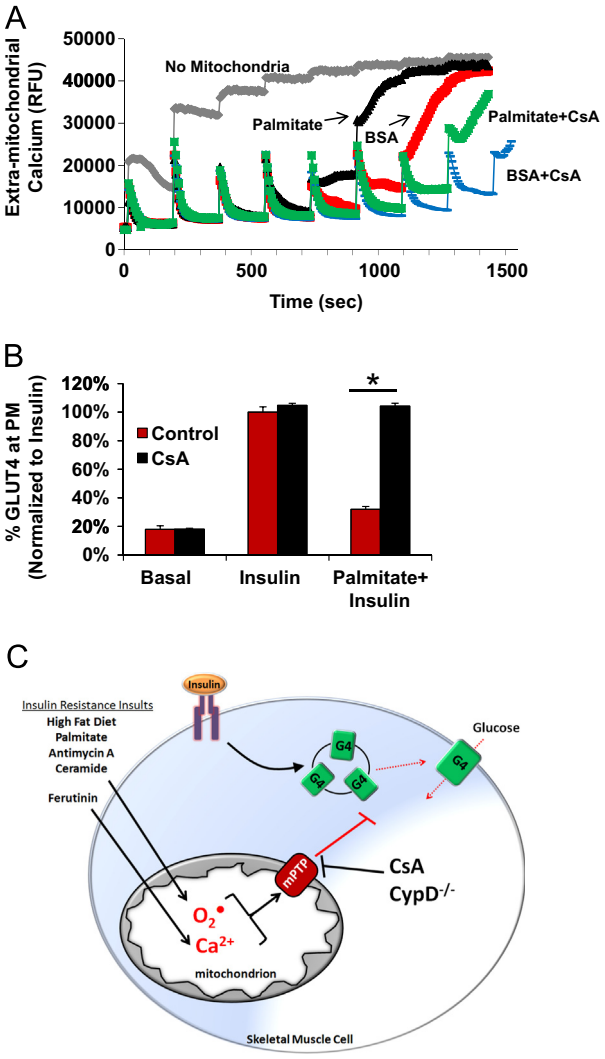

Figure 6: Palmitate-induced insulin resistance requires mPTP opening. (A) Calcium retention capacity was measured in mitochondria isolated from L6 myotubes treated for 16 h with 150 μM palmitate or control (BSA) in the absence or presence of CsA treatment (1 μg/mL). CsA improves mitochondrial calcium retention capacity in both palmitate- and BSA-treated cells. Representative traces are shown from one of three experiments that showed similar results. (B) Insulin-stimulated GLUT4 translocation to the PM was measured in control and palmitate-treated L6 myotubes in the absence or presence of CsA. Results are displayed as means ± SEM. $n=3$, $^*p<0.05$. (C) Opening of the mPTP promotes insulin resistance in skeletal muscle. Insults that promote excessive mitochondrial $O_2^{\bullet}$ and/or mitochondrial calcium overload converge on the mPTP to induce skeletal muscle insulin resistance, which is rescued by pharmacological or genetic inhibition of the mPTP.

muscle, but not in liver or adipose tissue. This tissue-specific phenotype may be the result of structural and physiological differences in the mPTP complex in skeletal muscle, compared to adipose and liver tissues. For example, skeletal muscle expresses the mPTP component ANT1, whereas the liver lacks ANT1, predominantly expresses ANT2 and has lower levels of ANT3 and ANT4 [35]. The tissue-specific isoforms of ANT also have distinct mitochondrial localization within the inner membrane [35] and contain subtle structural variations that may affect interactions between pore components. Supporting this notion, ANT1 is reported to have a higher binding affinity for CypD than ANT2 [35], and this CypD–ANT interaction promotes mPTP opening [18–21]. Another tissue-specific difference in mPTP composition involves HK2, which is expressed in skeletal muscle, but not in the liver. HK2 binds to the voltage-dependent anion channel (VDAC) in the mitochondrial outer membrane and stabilizes the structure to block mPTP opening [36,37], providing a molecular connection between glucose uptake and mPTP activity in skeletal muscle. Furthermore, this structural heterogeneity is known to dictate mPTP activity in response to metabolic stress, as the mPTP shows tissue-specific sensitivity to opening [38]. Therefore, variations in the composition and function of the mPTP may contribute to different pore dynamics in skeletal muscle and confer the tissue-specific regulation of insulin sensitivity.

Insulin resistance in muscle is frequently, but not always, associated with defects in the insulin signaling pathway. Our data demonstrate that mPTP opening promotes insulin resistance via a mechanism that does not involve alterations in the canonical insulin pathway. For example, induction of mPTP opening with insults that increase mitochondrial $O_2^{\bullet}$ and calcium caused insulin resistance at GLUT4 trafficking, but did not affect the insulin signaling pathway. Similarly, inhibition of mPTP opening did not improve insulin signal transduction *in vitro* or *in vivo*. This disconnect between insulin-stimulated GLUT4 trafficking and signaling through the canonical insulin pathway (*e.g.* IRS/PI3K/Akt/AS160) has been described by our group previously [2,22], and is in agreement with other studies showing that lipid-induced impairment in the formation of GLUT4 vesicles [39] and their translocation to the PM [34] do not involve altered signaling through the canonical pathway. This phenomenon is also observed in humans, where impaired muscle glucose transport in insulin resistant individuals or type 2 diabetes patients is not associated with defects in Akt activation [40,41]. In agreement with these previous studies, the data presented herein indicate that the mechanism linking mPTP opening to insulin resistance does not involve the canonical insulin signaling pathway through Akt.

The precise molecular mechanism whereby mPTP opening triggers insulin resistance is unclear, but the broad spectrum of mitochondrial ions and metabolites that escape the mitochondrial matrix during mPTP opening provides numerous possibilities. For example, calcium homeostasis is a critical function of mitochondria that is altered in insulin resistance. Normally, mitochondria serve as an intracellular calcium buffer to help maintain calcium homeostasis [42], with the mPTP opening transiently to act as a calcium release valve [19]. However, during periods of cellular stress, calcium accumulation in the mitochondrial matrix triggers high-conductance opening of the mPTP, which results in a loss of ionic gradients between the cytoplasm and mitochondrial matrix and an inability to retain matrix calcium [17,42]. Calcium retention capacity estimates the relative amount of calcium that mitochondria can store before undergoing mPTP opening and thus is a measure of both mPTP opening and mitochondrial quality [43]. In this study, we observed that high fat feeding reduces calcium retention capacity and sensitizes skeletal muscle mitochondria to mPTP opening, an effect that was reversed by deletion of CypD. However, apart from calcium [44], it is possible that blocking mPTP opening may sequester other ions such as iron [45,46] and metabolites such as fumarate [47] or acylcarnitines [48,49] that are associated with impaired insulin-stimulated glucose metabolism, and thus help maintain maximal insulin action in skeletal muscle. The identification of the precise molecules that pass through the mPTP to antagonize insulin action will require further elucidation.

It is thought that nutrient overload can alter mitochondrial shape [50], and insulin resistant skeletal muscle often contains swollen, misshapen mitochondria with damaged membranes [10,51]. In WT mice fed a HFD, we observe mitochondrial swelling and accumulation of damaged organelles in both intermyofibrillar and subsarcolemmal muscle regions, similar to the results seen by Bonnard et al. in mice fed a HFD for 16 weeks [10]. Remarkably, CypD KO muscle mitochondria were not swollen and demonstrated minimal evidence of damaged organelles compared to WT muscle. Our data therefore support findings of other groups which document that inhibition of CypD prevents mitochondrial swelling [23,52].

However, the molecular significance of mPTP-mediated swelling and regulation of muscle fiber morphology in the context of insulin resistance remains to be resolved.

In summary, our data show that opening of the mPTP is required for insulin resistance in skeletal muscle. This finding is important because it demonstrates a mechanism whereby mitochondrial dysfunction is causally linked to insulin resistance. Despite the question regarding whether mitochondrial dysfunction is a cause or consequence of insulin resistance [12], our current data suggest that in the early onset of diet-induced insulin resistance in skeletal muscle that mitochondrial dysfunction precedes impairment in insulin action. However, we acknowledge that our data do not rule out the possibility that insulin resistance may also occur upstream of mitochondrial dysfunction in different experimental conditions or genetic models. For example, the muscle insulin receptor knockout (MIRKO) mouse has skeletal muscle mitochondrial dysfunction [53]. Since mPTP opening is indicative of mitochondrial stress, one interpretation of the current data is that mPTP-induced insulin resistance represents an effort by the cell to decrease nutrient influx and reduce mitochondrial stress. This theory that insulin resistance may be a protective mechanism was originally hypothesized by Unger [54] and is supported by more recent studies [2,55–57]. Although insulin resistance may be protective in an acute setting, chronic insulin resistance promotes metabolic disease. Thus, the development of a muscle-specific mPTP inhibitor may have beneficial effects on glucose clearance in diabetics. Supporting this concept is the fact that metformin, one of the most effective anti-diabetes drugs, is a weak mPTP inhibitor [58] and improves skeletal muscle mitochondrial function and insulin sensitivity [59,60].

ACKNOWLEDGMENTS

This work was supported by the American Diabetes Association (ADA) Junior Faculty Award to KLH and an ADA basic science award to ZY.

CONFLICT OF INTEREST

The authors declare no conflicts of interest.

APPENDIX A. SUPPORTING INFORMATION

Supplementary data associated with this article can be found in the online version at http://dx.doi.org/10.1016/j.molmet.2013.11.003.

REFERENCES

[1] Holland, W.L., Knotts, T.A., Chavez, J.A., Wang, L.P., Hoehn, K.L., Summers, S.A., 2007. Lipid mediators of insulin resistance. Nutrition Reviews 65:S39–S46.

[2] Hoehn, K.L., Salmon, A.B., Hohnen-Behrens, C., Turner, N., Hoy, A.J., Maghzal, G. J., et al., 2009. Insulin resistance is a cellular antioxidant defense mechanism. Proceedings of the National Academy of Sciences of the United States of America 106:17787–17792.

[3] Murrow, B.A., Hoehn, K.L., 2010. Mitochondrial regulation of insulin action. International Journal of Biochemistry and Cell Biology 42:1936–1939.

[4] Savage, D.B., Petersen, K.F., Shulman, G.I., 2007. Disordered lipid metabolism and the pathogenesis of insulin resistance. Physiological Reviews 87:507–520.

[5] Houstis, N., Rosen, E.D., Lander, E.S., 2006. Reactive oxygen species have a causal role in multiple forms of insulin resistance. Nature 440:944–948.

[6] Anderson, E.J., Lustig, M.E., Boyle, K.E., Woodlief, T.L., Kane, D.A., Lin, C.T., et al., 2009. Mitochondrial h2o2 emission and cellular redox state link excess fat intake to insulin resistance in both rodents and humans. Journal of Clinical Investigation 119:573–581.

[7] Holland, W.L., Brozinick, J.T., Wang, L.P., Hawkins, E.D., Sargent, K.M., Liu, Y., et al., 2007. Inhibition of ceramide synthesis ameliorates glucocorticoid-, saturated-fat-, and obesity-induced insulin resistance. Cell Metabolism 5:167–179.

[8] Itani, S.I., Ruderman, N.B., Schmieder, F., Boden, G., 2002. Lipid-induced insulin resistance in human muscle is associated with changes in diacylglycerol, protein kinase c, and ikappab-alpha. Diabetes 51:2005–2011.

[9] Storlien, L.H., James, D.E., Burleigh, K.M., Chisholm, D.J., Kraegen, E.W., 1986. Fat feeding causes widespread in vivo insulin resistance, decreased energy expenditure, and obesity in rats. American Journal of Physiology 251: E576–E583.

[10] Bonnard, C., Durand, A., Peyrol, S., Chanseaume, E., Chauvin, M.A., Morio, B., et al., 2008. Mitochondrial dysfunction results from oxidative stress in the skeletal muscle of diet-induced insulin-resistant mice. Journal of Clinical Investigation 118:789–800.

[11] Petersen, K.F., Dufour, S., Befroy, D., Garcia, R., Shulman, G.I., 2004. Impaired mitochondrial activity in the insulin-resistant offspring of patients with type 2 diabetes. New England Journal of Medicine 350:664–671.

[12] Turner, N., Heilbronn, L.K., 2008. Is mitochondrial dysfunction a cause of insulin resistance? Trends in Endocrinology & Metabolism 19:324–330.

[13] Muoio, D.M., Neufer, P.D., 2012. Lipid-induced mitochondrial stress and insulin action in muscle. Cell Metabolism 15:595–605.

[14] Kim, J.A., Wei, Y., Sowers, J.R., 2008. Role of mitochondrial dysfunction in insulin resistance. Circulation Research 102:401–414.

[15] Giorgi, C., Agnoletto, C., Bononi, A., Bonora, M., De Marchi, E., Marchi, S., et al., 2012. Mitochondrial calcium homeostasis as potential target for mitochondrial medicine. Mitochondrion 12:77–85.

[16] Halestrap, A.P., Woodfield, K.Y., Connern, C.P., 1997. Oxidative stress, thiol reagents, and membrane potential modulate the mitochondrial permeability transition by affecting nucleotide binding to the adenine nucleotide translocase. Journal of Biological Chemistry 272:3346–3354.

[17] McStay, G.P., Clarke, S.J., Halestrap, A.P., 2002. Role of critical thiol groups on the matrix surface of the adenine nucleotide translocase in the mechanism of the mitochondrial permeability transition pore. Biochemical Journal 367:541–548.

[18] Zorov, D.B., Juhaszova, M., Yaniv, Y., Nuss, H.B., Wang, S., Sollott, S.J., 2009. Regulation and pharmacology of the mitochondrial permeability transition pore. Cardiovascular Research 83:213–225.

[19] Elrod, J.W., Molkentin, J.D., 2013. Physiologic functions of cyclophilin d and the mitochondrial permeability transition pore. Circulation Journal 77:1111–1122.

[20] Zhivotovsky, B., Galluzzi, L., Kepp, O., Kroemer, G., 2009. Adenine nucleotide translocase: a component of the phylogenetically conserved cell death machinery. Cell Death and Differentiation 16:1419–1425.

[21] Halestrap, A.P., 2009. What is the mitochondrial permeability transition pore? Journal of Molecular and Cellular Cardiology 46:821–831.

[22] Hoehn, K.L., Hohnen-Behrens, C., Cederberg, A., Wu, L.E., Turner, N., Yuasa, T., et al., 2008. Irs1-independent defects define major nodes of insulin resistance. Cell Metabolism 7:421–433.

[23] Baines, C.P., Kaiser, R.A., Purcell, N.H., Blair, N.S., Osinska, H., Hambleton, M.A., et al., 2005. Loss of cyclophilin d reveals a critical role for mitochondrial permeability transition in cell death. Nature 434:658–662.

[24] Hoehn, K.L., Turner, N., Swarbrick, M.M., Wilks, D., Preston, E., Phua, Y., et al., 2010. Acute or chronic upregulation of mitochondrial fatty acid oxidation has no net effect on whole-body energy expenditure or adiposity. Cell Metabolism 11:70–76.

[25] Patel, S.A., Hoehn, K.L., Lawrence, R.T., Sawbridge, L., Talbot, N.A., Tomsig, J.L., et al., 2012. Overexpression of the adiponectin receptor adipor1 in rat skeletal muscle amplifies local insulin sensitivity. Endocrinology 153:5231–5246.

[26] Murphy, R.C., James, P.F., McAnoy, A.M., Krank, J., Duchoslav, E., Barkley, R.M., 2007. Detection of the abundance of diacylglycerol and triacylglycerol molecular species in cells using neutral loss mass spectrometry. Analytical Biochemistry 366:59–70.

[27] Kim, H., Ahn, E., Moon, M.H., 2008. Profiling of human urinary phospholipids by nanoflow liquid chromatography/tandem mass spectrometry. Analyst 133: 1656–1663.

[28] Pulfer, M., Murphy, R.C., 2003. Electrospray mass spectrometry of phospholipids. Mass Spectrometry Reviews 22:332–364.

[29] Stuart, C.A., McCurry, M.P., Marino, A., South, M.A., Howell, M.E., Layne, A.S., et al., 2013. Slow-twitch fiber proportion in skeletal muscle correlates with insulin responsiveness. Journal of Clinical Endocrinology and Metabolism 98:2027–2036.

[30] Halestrap, A.P., Davidson, A.M., 1990. Inhibition of Ca-2+-induced large-amplitude swelling of liver and heart-mitochondria by cyclosporine is probably caused by the inhibitor binding to mitochondrial-matrix peptidyl-prolyl cis-trans isomerase and preventing it interacting with the adenine-nucleotide translocase. Biochemical Journal 268:153–160.

[31] Macho, A., Blanco-Molina, M., Spagliardi, P., Appendino, G., Bremner, P., Heinrich, M., et al., 2004. Calcium ionophoretic and apoptotic effects of ferutinin in the human jurkat t-cell line. Biochemical Pharmacology 68:875–883.

[32] Abramov, A.Y., Duchen, M.R., 2003. Actions of ionomycin, 4-bra23187 and a novel electrogenic Ca2+ ionophore on mitochondria in intact cells. Cell Calcium 33:101–112.

[33] Garcia-Ruiz, C., Colell, A., Mari, M., Morales, A., Fernandez-Checa, J.C., 1997. Direct effect of ceramide on the mitochondrial electron transport chain leads to generation of reactive oxygen species. Role of mitochondrial glutathione. Journal of Biological Chemistry 272:11369–11377.

[34] Chiu, T.T., Sun, Y., Koshkina, A., Klip, A., 2013. Rac-1 superactivation triggers insulin-independent glucose transporter 4 (glut4) translocation that bypasses signaling defects exerted by c-jun n-terminal kinase (jnk)- and ceramide-induced insulin resistance. Journal of Biological Chemistry 288:17520–17531.

[35] Vyssokikh, M.Y., Katz, A., Rueck, A., Wuensch, C., Dorner, A., Zorov, D.B., et al., 2001. Adenine nucleotide translocator isoforms 1 and 2 are differently distributed in the mitochondrial inner membrane and have distinct affinities to cyclophilin d. Biochemical Journal 358:349–358.

[36] Arora, K.K., Filburn, C.R., Pedersen, P.L., 1993. Structure/function relationships in hexokinase. Site-directed mutational analyses and characterization of over-expressed fragments implicate different functions for the n- and c-terminal halves of the enzyme. Journal of Biological Chemistry 268:18259–18266.

[37] Wu, R., Wyatt, E., Chawla, K., Tran, M., Ghanefar, M., Laakso, M., et al., 2012. Hexokinase ii knockdown results in exaggerated cardiac hypertrophy via increased ros production. EMBO Molecular Medicine 4:633–646.

[38] Endlicher, R., Krivakova, P., Lotkova, H., Milerova, M., Drahota, Z., Cervinkova, Z., 2009. Tissue specific sensitivity of mitochondrial permeability transition pore to Ca^{2+} ions. Acta Medica (Hradec Kralove) 52:69–72.

[39] Tsuchiya, Y., Hatakeyama, H., Emoto, N., Wagatsuma, F., Matsushita, S., Kanzaki, M., 2010. Palmitate-induced down-regulation of sortilin and impaired glut4 trafficking in c2c12 myotubes. Journal of Biological Chemistry 285: 34371–34381.

[40] Kim, Y.B., Nikoulina, S.E., Ciaraldi, T.P., Henry, R.R., Kahn, B.B., 1999. Normal insulin-dependent activation of akt/protein kinase b, with diminished activation of phosphoinositide 3-kinase, in muscle in type 2 diabetes. Journal of Clinical Investigation 104:733–741.

[41] Frojdo, S., Vidal, H., Pirola, L., 2009. Alterations of insulin signaling in type 2 diabetes: a review of the current evidence from humans. Biochimica et Biophysica Acta 1792:83–92.

[42] Patergnani, S., Suski, J.M., Agnoletto, C., Bononi, A., Bonora, M., De Marchi, E., et al., 2011. Calcium signaling around mitochondria associated membranes (mams). Cell Communication and Signaling 9:19.

[43] Teodoro, J.S., Duarte, F.V., Gomes, A.P., Varela, A.T., Peixoto, F.M., Rolo, A.P., et al., 2013. Berberine reverts hepatic mitochondrial dysfunction in high-fat fed rats: a possible role for sirt3 activation. Mitochondrion 13:637–646.

[44] Zemel, M.B., 1998. Nutritional and endocrine modulation of intracellular calcium: implications in obesity, insulin resistance and hypertension. Molecular and Cellular Biochemistry 188:129–136.

[45] Han, D.H., Hancock, C.R., Jung, S.R., Higashida, K., Kim, S.H., Holloszy, J.O., 2011. Deficiency of the mitochondrial electron transport chain in muscle does not cause insulin resistance. PLoS One 6:e19739.

[46] Fernandez-Real, J.M., Lopez-Bermejo, A., Ricart, W., 2002. Cross-talk between iron metabolism and diabetes. Diabetes 51:2348–2354.

[47] Frizzell, N., Lima, M., Baynes, J.W., 2011. Succination of proteins in diabetes. Free Radical Research 45:101–109.

[48] Koves, T.R., Ussher, J.R., Noland, R.C., Slentz, D., Mosedale, M., Ilkayeva, O., et al., 2008. Mitochondrial overload and incomplete fatty acid oxidation contribute to skeletal muscle insulin resistance. Cell Metabolism 7:45–56.

[49] Schooneman, M.G., Vaz, F.M., Houten, S.M., Soeters, M.R., 2013. Acylcarnitines: reflecting or inflicting insulin resistance? Diabetes 62:1–8.

[50] Galloway, C.A., Yoon, Y.S., 2012. What comes first, misshape or dysfunction? The view from metabolic excess. Journal of General Physiology 139:455–463.

[51] Zhang, X., Wang, C., Song, G., Gan, K., Kong, D., Nie, Q., et al., 2013. Mitofusion-2-mediated alleviation of insulin resistance in rats through reduction in lipid intermediate accumulation in skeletal muscle. Journal of Biomedical Science 20:45.

[52] Hansson, M.J., Morota, S., Chen, L., Matsuyama, N., Suzuki, Y., Nakajima, S., et al., 2011. Cyclophilin d-sensitive mitochondrial permeability transition in adult human brain and liver mitochondria. Journal of Neurotrauma 28:143–153.

[53] Franko, A., von Kleist-Retzow, J.C., Bose, M., Sanchez-Lasheras, C., Brodesser, S., Krut, O., et al., 2012. Complete failure of insulin-transmitted signaling, but not obesity-induced insulin resistance, impairs respiratory chain function in muscle. Journal of Molecular Medicine (Berlin) 90:1145–1160.

[54] Unger, R.H., 2003. Lipid overload and overflow: metabolic trauma and the metabolic syndrome. Trends in Endocrinology and Metabolism 14:398–403.

[55] Nunn, A.V., Bell, J.D., Guy, G.W., 2009. Lifestyle-induced metabolic inflexibility and accelerated ageing syndrome: insulin resistance, friend or foe? Nutrition and Metabolism (London) 6:16.

[56] Harmancey, R., Lam, T.N., Lubrano, G.M., Guthrie, P.H., Vela, D., Taegtmeyer, H., 2012. Insulin resistance improves metabolic and contractile efficiency in stressed rat heart. FASEB Journal 26:3118–3126.

[57] Barzilai, N., Ferrucci, L., 2012. Insulin resistance and aging: a cause or a protective response? Journals of Gerontology Series A: Biological Sciences and Medical Sciences 67:1329–1331.

[58] Guigas, B., Detaille, D., Chauvin, C., Batandier, C., De Oliveira, F., Fontaine, E., et al., 2004. Metformin inhibits mitochondrial permeability transition and cell death: a pharmacological in vitro study. Biochemical Journal 382:877–884.

[59] Suwa, M., Egashira, T., Nakano, H., Sasaki, H., Kumagai, S., 2006. Metformin increases the pgc-1alpha protein and oxidative enzyme activities possibly via ampk phosphorylation in skeletal muscle in vivo. Journal of Applied Physiology (1985) 101:1685–1692.

[60] Rossetti, L., DeFronzo, R.A., Gherzi, R., Stein, P., Andraghetti, G., Falzetti, G., et al., 1990. Effect of metformin treatment on insulin action in diabetic rats: in vivo and in vitro correlations. Metabolism 39:425–435.

